

Electronic Supplementary Material (ESI) for Journal of Materials Chemistry A.

This journal is © The Royal Society of Chemistry 2020

Supporting Information

Cotton Pad-derived Large-area 3D N-doped Graphene-like Full Carbon Cathode with O-rich Functional Group for Flexible All Solid Zn-air Batteries

Xiangjun Zheng^a, Xuecheng Cao^a, Kai Zeng^a, Zhihui Sun^a, Jin Yan^a, Xiaowei Li^a, Chao Jin^{a,*},
Xin Chen^{b,*}, and Ruizhi Yang^{a,*}

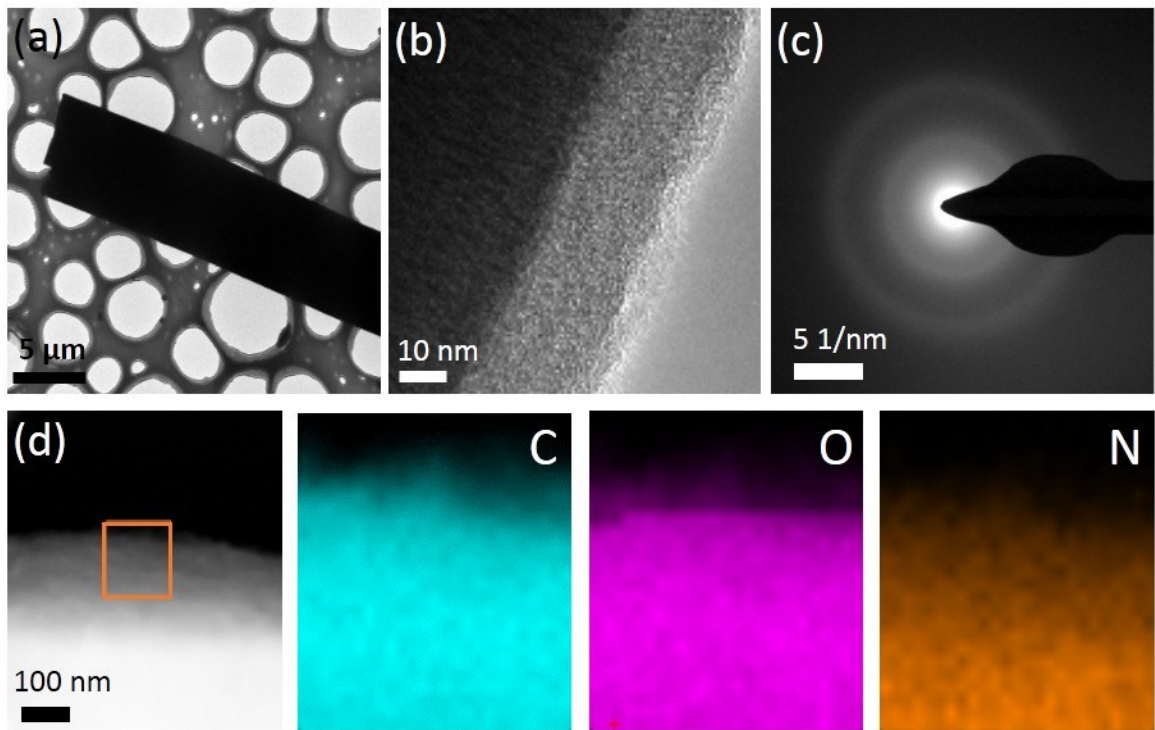
^a College of Energy, Soochow Institute for Energy and Materials Innovations, Soochow University, Suzhou, 215006, China

^b Center for Computational Chemistry and Molecular Simulation, College of Chemistry and Chemical Engineering, Southwest Petroleum University, Chengdu 610500, China

*Corresponding Authors: E-mail: jinchao@suda.edu.cn (C. Jin); yangrz@suda.edu.cn (R Yang);
chenxin830107@pku.edu.cn (X. Chen)

Figure S1-S17

Table S1-S4



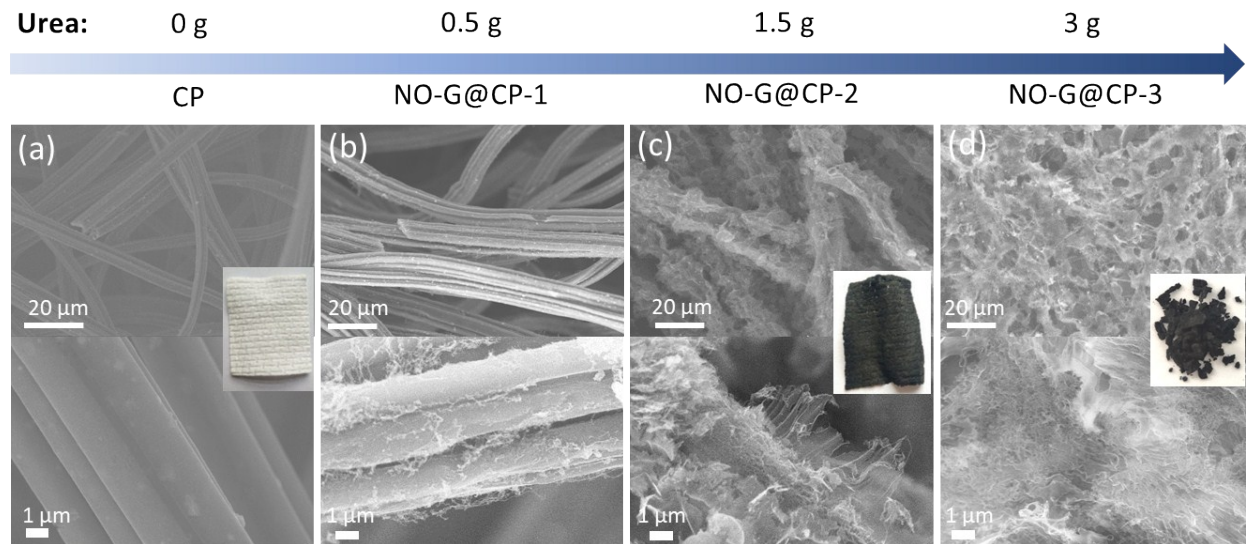
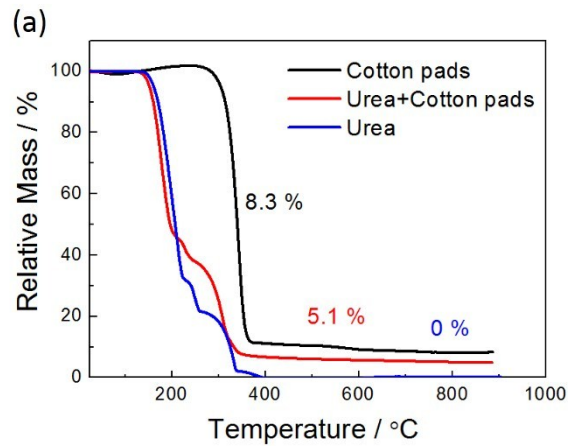
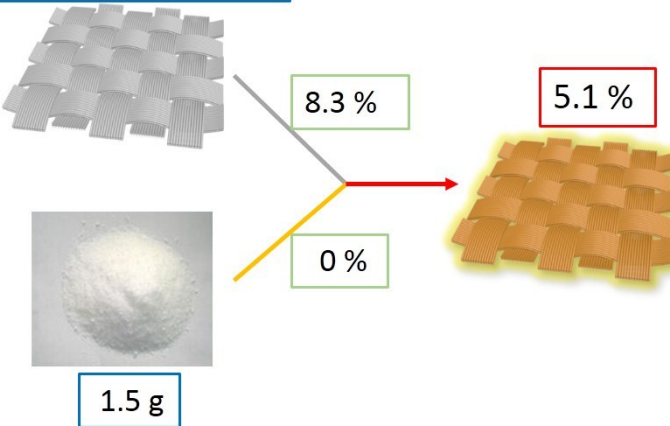


Fig. S2. SEM image of CP (a), NO-G@CP-1 (b), NO-G@CP-2 (c) and NO-G@CP-3 (d).



(b) $0.2642 \text{ g} / 5 * 5.5 \text{ cm}^2$



(c)

$$\frac{0.2642\text{g}*8.3\%+1.5\text{g}*0\%}{0.2642\text{g}+1.5\text{g}} = 1.2\% < \boxed{5.1\%}$$

Fig. S3. (a) TGA of urea, cotton pad and the mixture of urea and cotton pad. (b and c) Diagram and compute of the comparison for TGA.

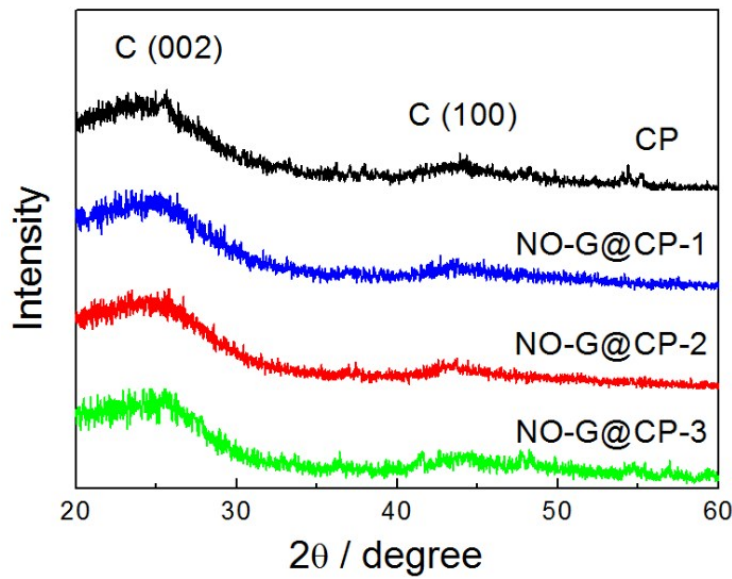


Fig. S4. XRD pattern of as-prepared samples.

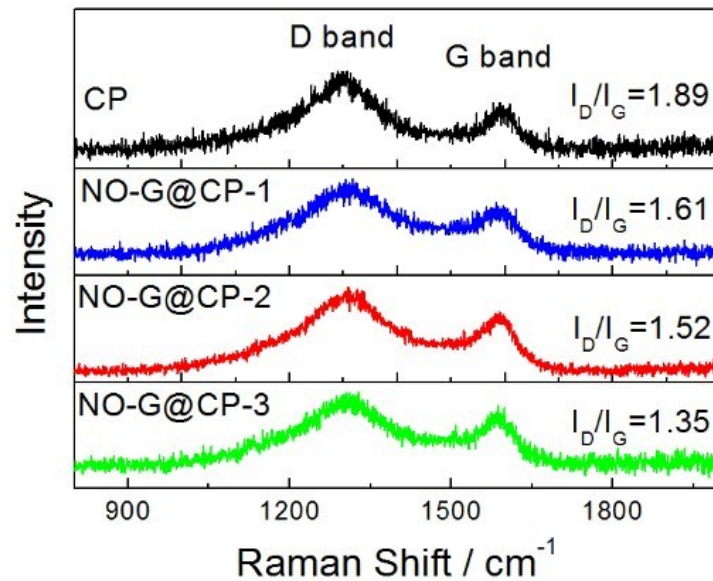


Fig. S5. Raman spectra of as-prepared samples.

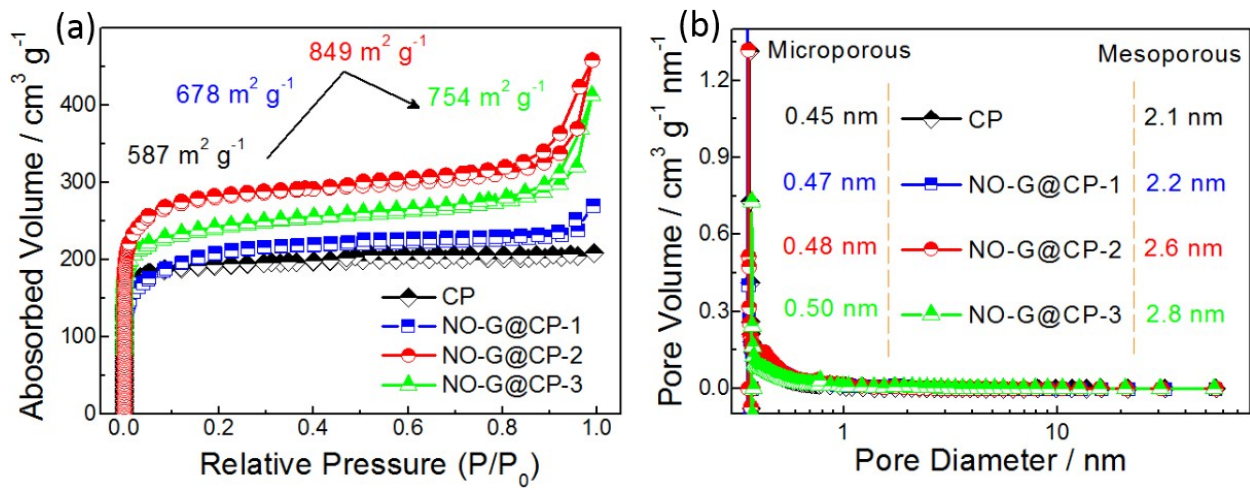


Fig. S6. (a) Nitrogen adsorption and desorption isotherms of as-prepared samples. (b) Pore-size distributions of as-prepared samples.

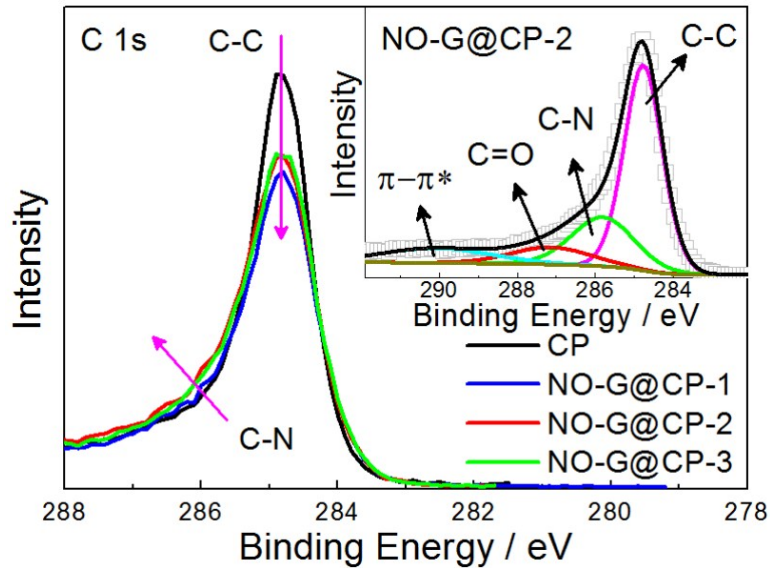


Fig. S7. The high-resolution XPS spectra for C 1 s of CP, NO-G@CP-1, NO-G@CP-2 and NO-G@CP-3.

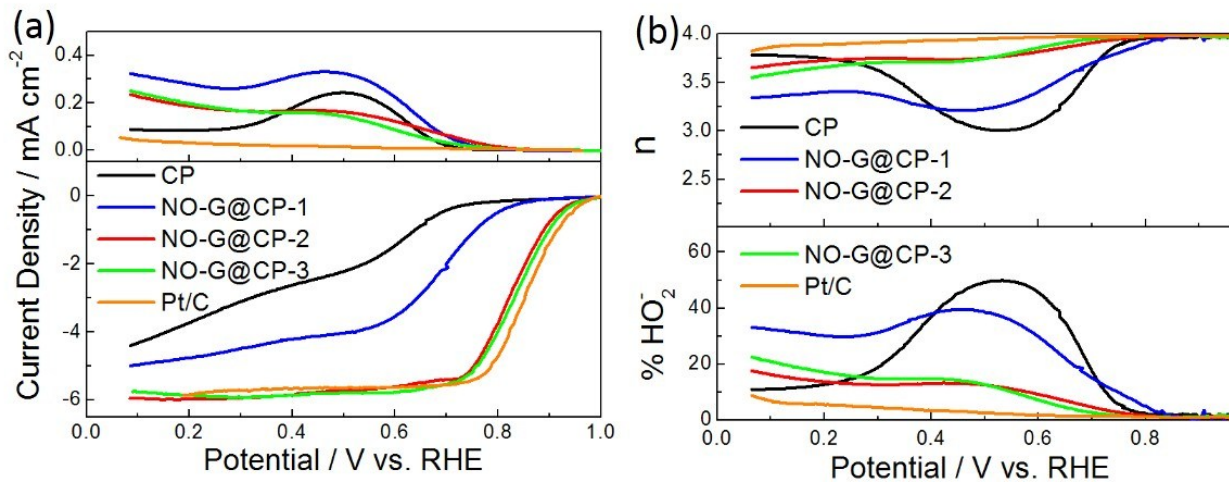


Fig. S8. (a) Disk (I_D) and ring (I_R) current density of ORR obtained with LSVs on RRDE for prepared samples and commercial Pt/C (20 wt%). (b) Calculated electron transfer number (n) and peroxide yield (% HO_2^-) based on the corresponding RRDE data.

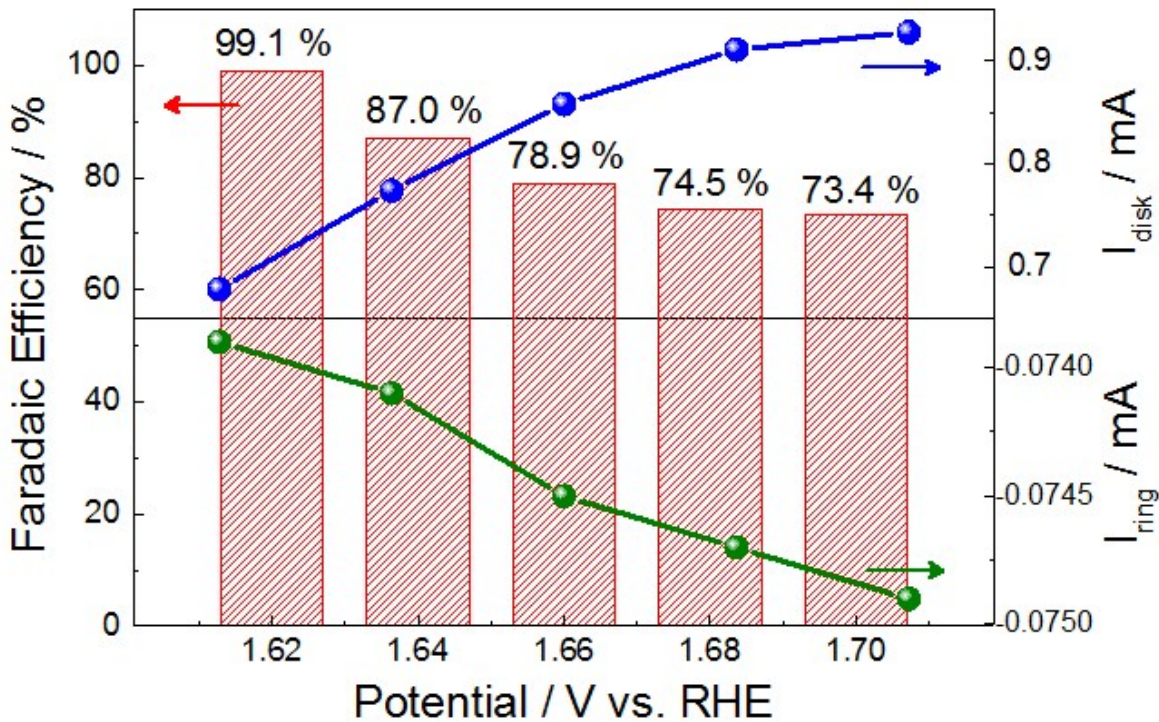


Fig. S9. Faradaic efficiency of NO-G@CP-2 catalyst in 0.1 M KOH at 1600 rpm under N₂ saturation.

The disk electrode was maintained at constant potential steps from 1.62 to 1.70 V for consecutive periods of 1 min each, and the ring electrode was held at 0.2 V. The Faradaic efficiency can be calculated as: Faradaic efficiency = $2I_{\text{ring}} / NI_{\text{disk}}$, where I_{ring} and I_{disk} are the measured ring and disk currents, respectively, and N is the collection efficiency of RRDE, 0.22 in this work.

Fig. S9 shows the disk and ring currents, and the corresponding Faradaic efficiency of the NO-G@CP-2 catalyst as a function of applied disk potential. The highest Faradaic efficiency is 99.1% at the applied disk potential of 1.62 V, and decreases to 73.4% with the disk voltage increasing to 1.70 V. This decreasing Faradaic efficiency can be ascribed to apparently large amounts of undissolved oxygen bubbles generated at the relatively high applied disk potentials, which might not be collected efficiently by the Pt ring electrode. Therefore, the Faradaic efficiency of 99.1% achieved at 1.62 V has been presented as the OER efficiency of the NO-G@CP-2 catalyst because this disk current density (3.46 mA cm^{-2}) is adequately high to generate oxygen.

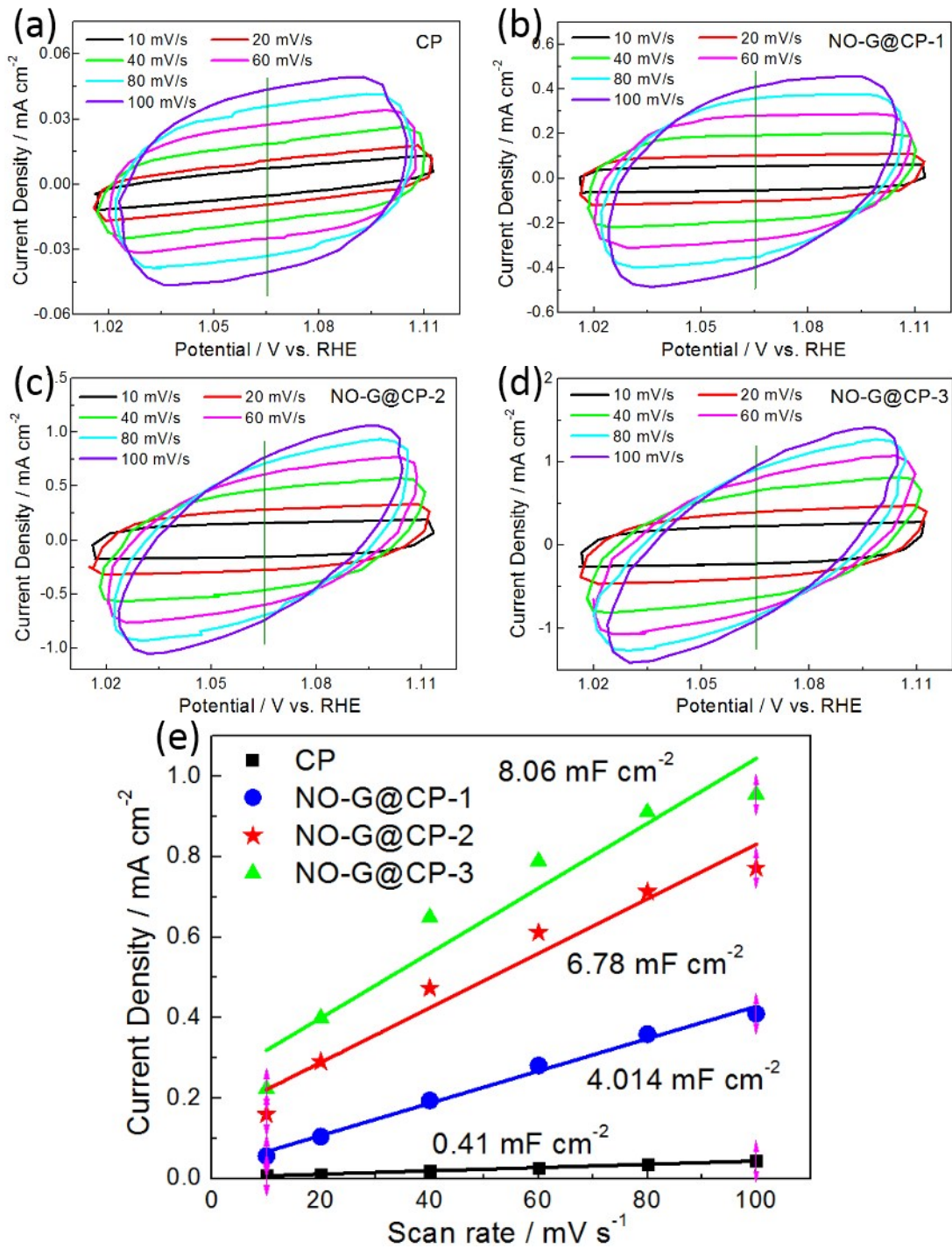


Fig.S10. CV curves in the region of 1.0-1.1 V at scan rates from 10 to 100 mV s⁻¹ and corresponding linear fitting of capacitive current for CP, NO-G@CP-1, NO-G@CP-2 and NO-G@CP-3.



Fig. S11. Photograph of wearable device powered by two flexible Zn-air batteries with the NO-G@CP-2 as the air cathode connected in series.

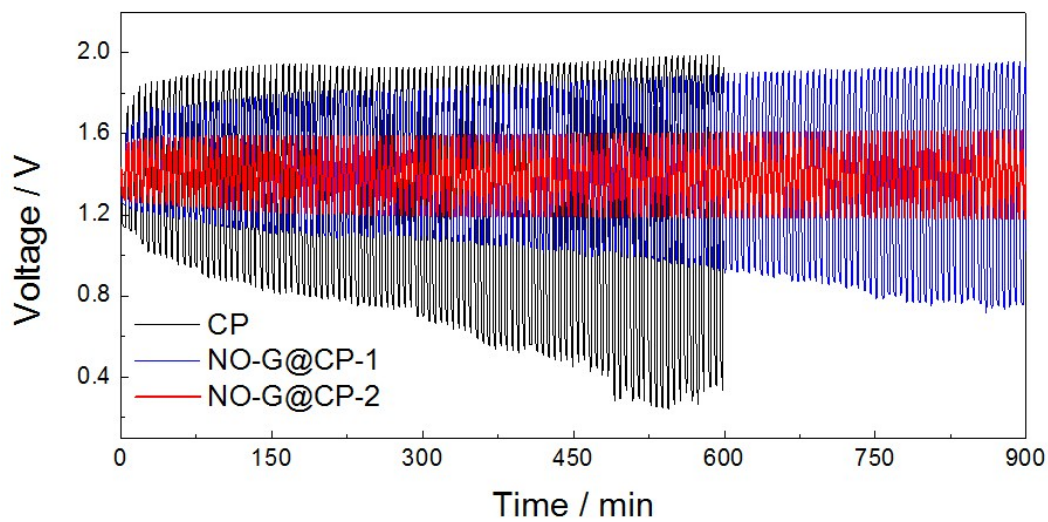


Fig. S12. Long-term cycling performances at current density of 2.0 mA cm⁻² for FASS ZAB based on CP, NO-G@CP-1 and NO-G@CP-2, respectively.

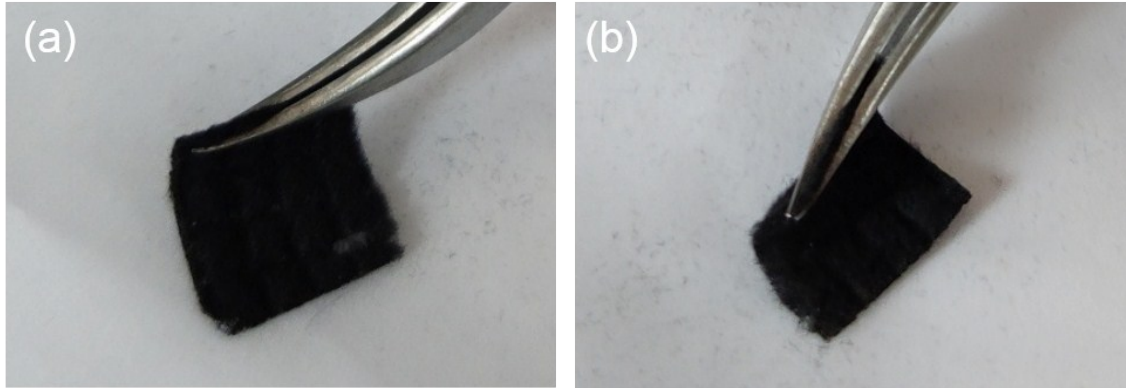


Fig. S13. Photograph of NO-G@CP-2 catalyst sheet that was stripped off from flexible ZAB after a long-term discharge-charge test.

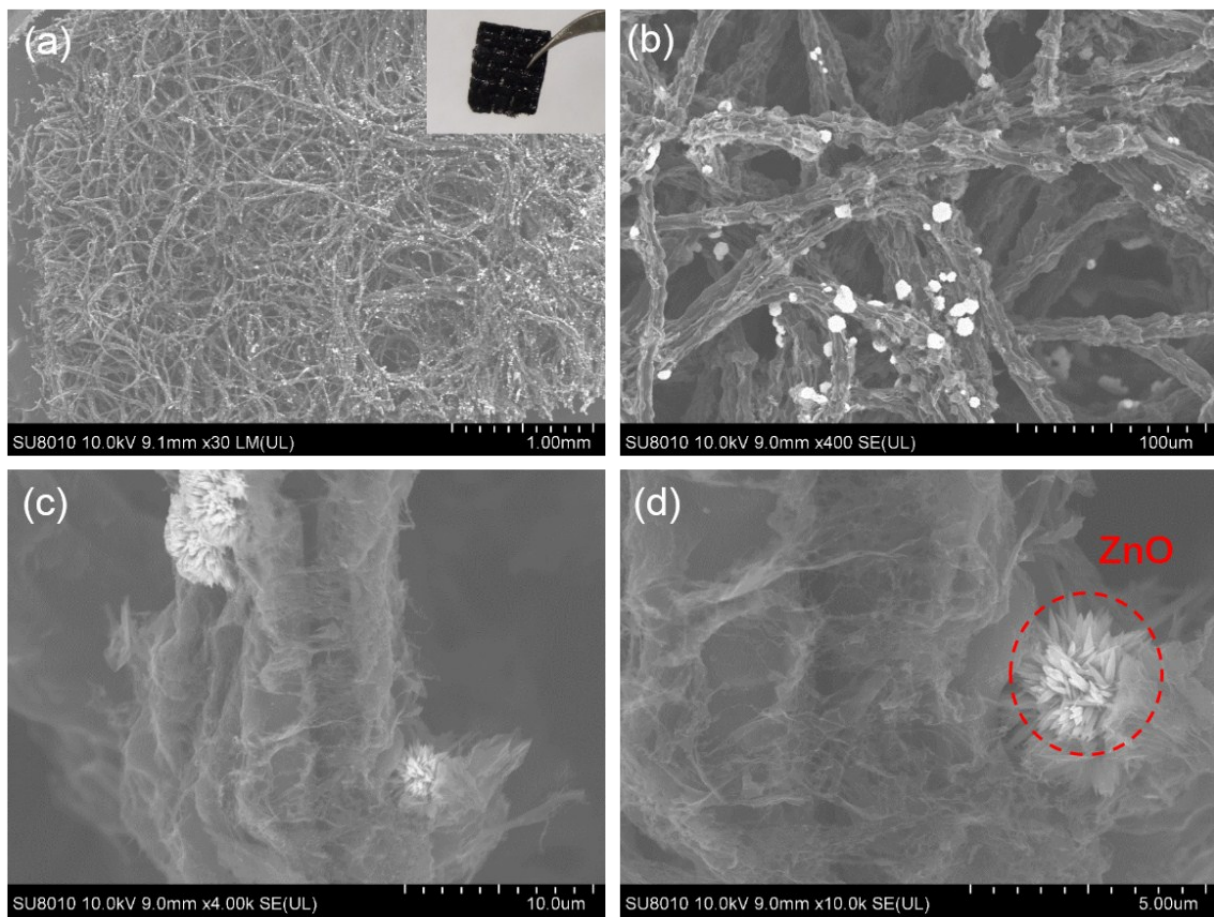


Fig. S14. SEM images of NO-G@CP-2 after long-term discharge-charge test for FASS ZAB.

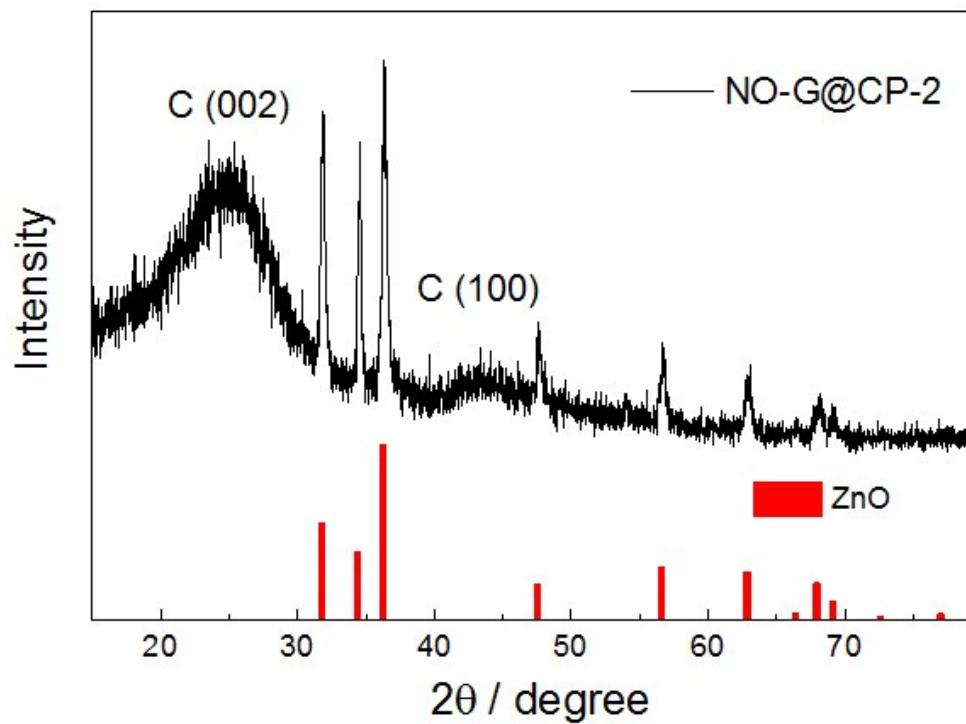


Fig. S15. XRD pattern of NO-G@CP-2 after long-term discharge-charge test for FASS ZAB.

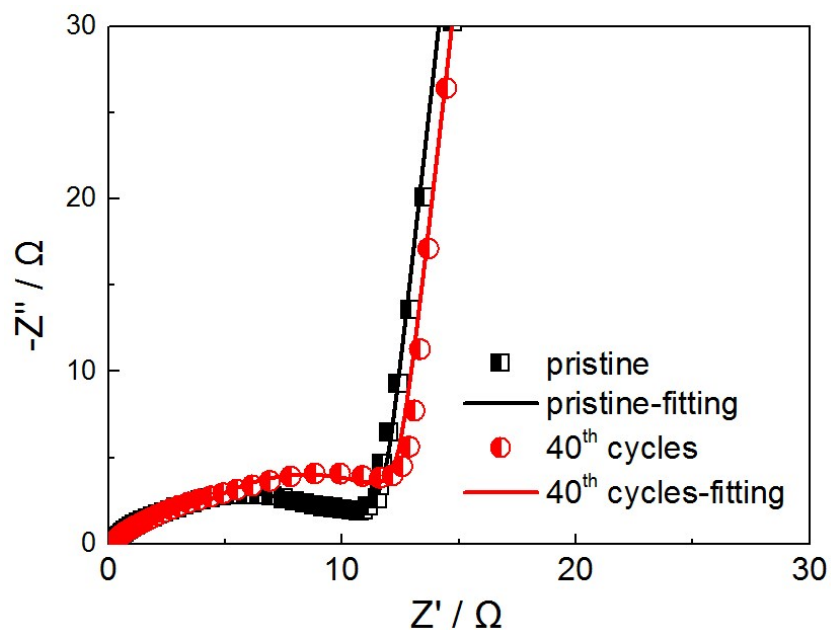


Fig. S16. Nyquist plots of the impedance of FASS ZAB based on NO-G@CP-2 in pristine and after a long-cycle life with bending at a potential of 1.43 V.

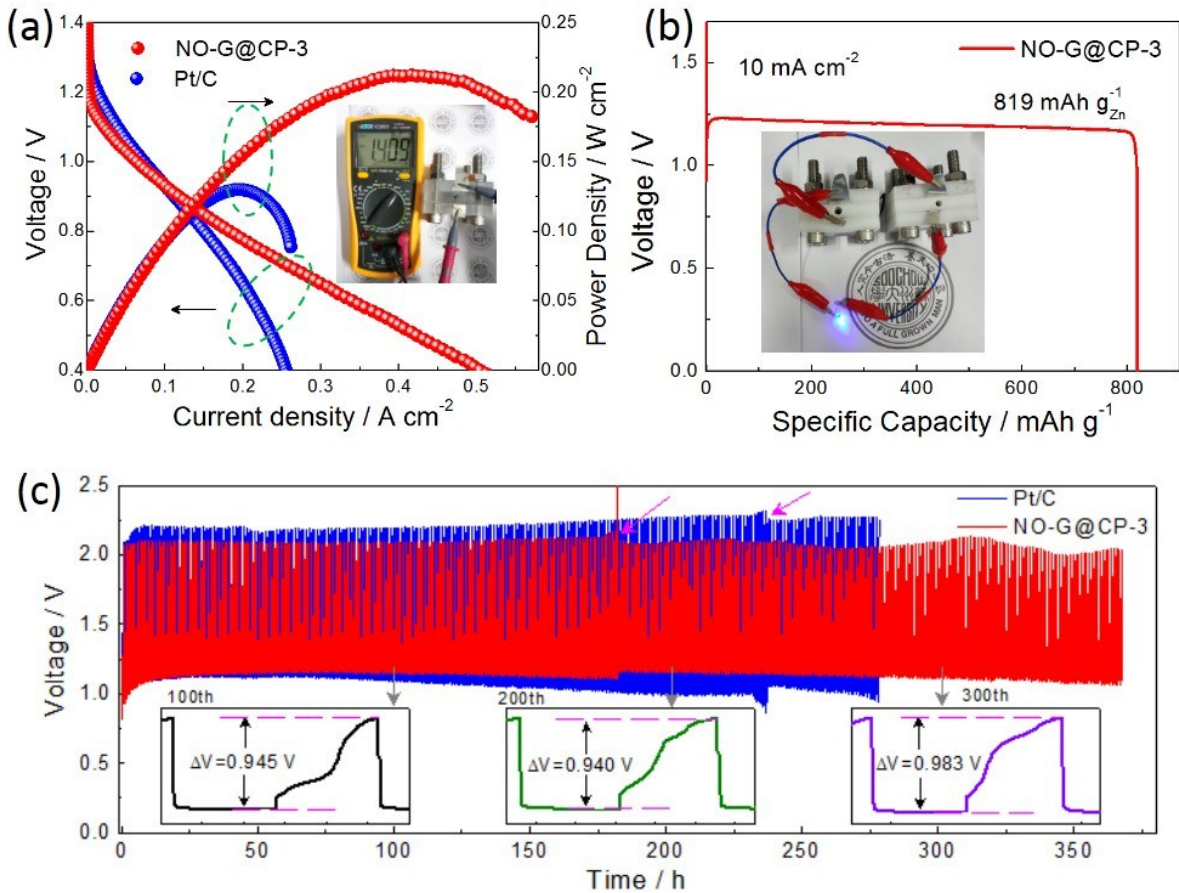


Fig. S17. (a) I-V and I-P curves of NO-G@CP-3 and commercial Pt/C based ZABs. (b) Long-term galvanostatic discharge curve of NO-G@CP-3 based liquid ZAB. (c) Discharge-charge stabilities of NO-G@CP-3 and commercial Pt/C at a current density of 10 mA cm^{-2} .

As anticipated, a high open-circuit voltage (1.409 V), a maximum power density of 212 mW cm^{-2} with a cutoff current density of 520 mA cm^{-2} are obtained (Fig. S11a), which is 162 % of ZABs based on commercial Pt/C electrocatalysts (131 mW cm^{-2}). At a current density of 10 mA cm^{-2} , the ZAB sustains a constant voltage of ca. 1.25 V for over 30 h to generate a specific capacity of $819 \text{ mAh g}_{\text{Zn}}^{-1}$ normalized to the mass of consumed Zn, which is closely to the theoretical capacity of $820 \text{ mAh g}_{\text{Zn}}^{-1}$, and corresponds to a high energy density of $983 \text{ Wh kg}_{\text{Zn}}^{-1}$ ($\approx 90.5\%$ of the theoretical energy density of $1086 \text{ Wh kg}_{\text{Zn}}^{-1}$). Based on the outstanding performance, a blue LED lamp could be continuously lightened by two series-connected liquid ZABs (Fig. S11b). The discharge-charge stability is also characterized at 10 mA cm^{-2} and presented in Fig. S11c. Except for occasional voltage jump due to supplying new electrolyte (as shown with the red arrowhead), NO-G@CP-3 based ZABs delivers a stable discharge-charge voltage gap of 0.94-

0.98 V after 360 cycles, which is much smaller than that of Pt/C based ZABs. The performance is also similar to and/or even smaller than that of some reported liquid ZABs (Table S4). Although NO-G@CP-3 cannot be used in flexible devices, it is well applied to liquid ZABs.

Table S1. The different O species derived from fitted peak O 1s obtained from XPS for recently reported oxygen-rich materials.

Catalyst	O%	Fitted peaks	Reference
O-CNTs	8.2	Absorbed O, C=O, C-O	S1
P-CC	13.09	COO- and O=C-O, C-OH and C=O, O=C-O, H-O-H	S2
O-NGM	6.97	Absorbed O, C=O, O-C	S3
CC-AC	6.3	C=O,C-OH,O-C=O,COOH	S4
NO-G@CP	6.7	Absorbed O, C=O, C-O	This work

Table S2. The electrocatalytic activities of the recently reported carbon-based bifunctional catalysts for ORR and OER.

Catalyst	Catalyst loading (mg cm ⁻²)	E _{onset} (V vs. RHE)	E _{1/2 j=-3} (V vs. RHE)	E _{j=10} (V vs. RHE)	IR corrected	Reference
NiCo@N-C	0.4	0.90	0.81	1.76	-	S5
Co₂P/CoN-in-NCNTs	0.1	0.91	0.84	1.75	IR	S6
Co₉S₈/NSPC9-45	0.25	0.89	0.75	1.55	-	S7
Co-N-CNTs	0.81	1.0	0.9	1.7	-	S8
NGM-Co	0.25	0.85	0.7	1.75	IR	S9
N-GCNT/FeCo	0.2	1.0	0.9	1.73		S10
N-RGO	0.6	0.87	0.7	1.71	IR	S11
NCNF	0.1	0.95	0.8	1.86	IR	S12
S,N-Fe/N/C-CNT	0.6	0.92	0.83	1.6	IR	S13
S,N-C-CNT	0.6	0.82	0.55	1.8	IR	
NO-G@CP-2	0.4	0.95	0.83	1.73	IR	This work
NO-G@CP-3	0.4	0.95	0.84	1.83	IR	This work

Table S3. The performance of flexible rechargeable Zn-air batteries with various bifunctional electrocatalysts.

Electrode material	Additive	V_{Open} / V	Power density	Current Density	Period / min Cycling time / h Cycling number	η / V	Reference
NO-G@CP-2	free-standing	1.328	65.1 mW cm⁻²	2 mA cm⁻²	6 / 18 / 180	0.43	This work
CC-AC	binder-free	1.367	52.3 mW cm ⁻³	1 mA cm ⁻²	20 / 16.7 / 50	0.98	S4
N,S-CC	additive-free	1.247	62 mW cm ⁻³	5 mA cm ⁻³	4 / 8 / 120	1.2	S14
NCNF	free-standing	1.256	-	2 mA cm ⁻²	10 / 6 / 36	0.78	S15
NPCS-900	Loaded on CC	1.40	55 mW cm ⁻²	1 mA cm ⁻²	- /30 /-	1	S16
silkNC/KB	Loaded on CC	-	32.3 mW cm ⁻²	1 mA cm ⁻²	- /- /30	1.1	S17
N-CNTf-170	free-standing	1.31	-	-	20/1/3	1.1	S18
Co-NC@Al₂O₃-ZABs	binder-free	1.41	72.4 mW cm ⁻³	20 mA cm ⁻³	10 / 10 / 60	0.91	S19
MoOx-GCC	binder-free	1.427	32 mW cm ⁻²	0.7 mA cm ⁻²	20 / 67 / 200	0.7	S20
P-CoSe₂/N-C FAs	Loaded on CC	1.30	-	1 mA cm ⁻²	20 / 26.7 / 50	0.95	S21
NC-Co₃O₄	Loaded on CC	1.44	82 mW cm ⁻³	1 mA cm ⁻²	20 / 20 / 60	1	S22
CNT@COF	free-standing	1.39	22.3 mW cm ⁻²	1 mA cm ⁻²	- /- /12	0.75	S23
Co-FeCo/N-G	free-standing	1.419	82 mW cm ⁻²	1 mA cm ⁻²	10/18/108	0.7	S24
Co-SAs@NC	Loaded on CC	1.40	-	2 mA cm ⁻²	20/11.67/35	1.25	S25
1 nm-CoO_x	Loaded on CC	1.39	120 mW cm ⁻²	6 mA cm ⁻²	10/10/60	0.57	S26

Table S4. The comparative performance of carbon-based rechargeable Zn-air batteries using liquid alkaline electrolytes.

Electrode material	Loading /mg cm ⁻²	Power density/ mW cm ⁻²	Capacity / mAh g _{Zn} ⁻¹	I/mA cm ⁻²	Period / min Cycling time / h Cycling number	$\eta_{\text{initial}}/\eta_{\text{end}}$ / V	Reference
NO-G@CP-3	1	212	819	10	60 / 370 / 370	1.23/0.95	This work
NCNF	2	185	626	10	10 / 83 /500	0.73 / 0.86	S12
N,S-CC	-	-	715	20	- / - / 240	1.2 / 1.21	S14
NDGs	1	115	751	10	20 / 78 / 234	0.87 / 1.07	S15
N/S-2DPC	3	0.69	-	20	10 / 12 / 72	0.84 / 0.88	S27
NOGB	1	112	-	10	- / 30 / -	1.18 / 1.19	S28
NPCS-900	-	79	684	2	10/55/337	1.1/0.9	S16
silkNC/KB	1	91.2	614.7	10	20/33/100	0.81/1.03	S17
NSG@CNT-2	1	188	800	10	10/33/200	0.8/1.1	S29
O-N-CNs/CP	1	89	660	10	20/24/72	1.1/1.2	S30
NOGB-800	1	111.9	-	10	20/30/	1.1/1.25	S31
BN-GAs-2	1	-	520	10	11.1/22.2/200	1.2/0.8	S32
Co₂P/CoN-NCNT_S	0.5	195	650	5	120 / 84 / 42	0.82 / 1.1	S6
Co-N-CNT	1	101	-	2	6.67 / 16 / 144	0.8 / 1.33	S8
Co₃O₄/CC	2.72	41	743	1	30 / 100 / 200	1.1 / 0.9	S33
C-CoPAN	1	125	-	1	60 / 135 / 135	0.7 / 0.78	S34
Co₄N/CNW/C	-	174	774	10	20 / 136 / 408	0.84 / 0.87	S35
egg-CMS	3.2	-	-	6.4	- / - / 30	0.56 / 1.17	S36
FeCo-Co₄N/N-C	1	11.4	-	2	10 / 72 / 432	0.87 / 0.93	S37
Fe/N/C@BMZ IF	1	235	-	10	10 / 17 / 100	0.82 / 0.85	S38

Reference

- S1. L. Q. Li, H. B. Yang, J. W. Miao, L. P. Zhang, H. Y. Wang, Z. P. Zeng, W. Huang, X. C. Dong, B. Liu. Unraveling Oxygen Evolution Reaction on Carbon-Based Electrocatalysts: Effect of Oxygen Doping on Adsorption of Oxygenated Intermediates. *ACS Energy Lett.*, 2017, **2**, 294-300.
- S2. Z. J. Liu, Z. H. Zhao, Y. Y. Wang, S. Dou, D. F. Yan, D. D. Liu, Z. H. Xia, S. Y. Wang, In Situ Exfoliated, Edge-Rich, Oxygen-Functionalized Graphene from Carbon Fibers for Oxygen Electrocatalysis. *Adv. Mater.*, 2017, **29**, 1606207.
- S3. M. F. Wang, W. P. Wang, T. Qian, S. S. Liu, Y. T. Li, Z. F. Hou, J. B. Goodenough, P. M. Ajayan, C. L. Yan, Oxidizing Vacancies in Nitrogen-Doped Carbon Enhance Air-Cathode Activity. *Adv. Mater.*, 2019, **31**, 1803339.
- S4. K. Kordek, L. X. Jiang, K. C. Fan, Z. J. Zhu, Li Xu, M. Al-Mamun, Y. H. Dou, S. Chen, P. R. Liu, H. J. Yin, P. Rutkowski, H. J. Zhao, Two-Step Activated Carbon Cloth with Oxygen-Rich Functional Groups as a High-Performance Additive-Free Air Electrode for Flexible Zinc-Air Batteries. *Adv. Energy Mater.*, 2019, **9**, 1802936.
- S5. Y. Fu, H.-Y. Yu, C. Jiang, T.-H. Zhang, R. Zhan, X. Li, J.-F. Li, J.-H. Tian, R. Yang, NiCo Alloy Nanoparticles Decorated on N-Doped Carbon Nanofibers as Highly Active and Durable Oxygen Electrocatalyst. *Adv. Funct. Mater.*, 2018, **28**, 1705094.
- S6. Y. Y. Guo, P. F. Yuan, J. N. Zhang, H. C. Xia, F. Y. Cheng, M. F. Zhou, J. Li, Y. Y. Qiao, S. C. Mu, Q. Xu, Co₂P-CoN Double Active Centers Confined in N-Doped Carbon Nanotube: Heterostructural Engineering for Trifunctional Catalysis toward HER, ORR, OER, and Zn-Air Batteries Driven Water Splitting. *Adv. Funct. Mater.*, 2018, **28**, 1805641.
- S7. H.-X. Zhong, K. Li, Q. Zhang, J. Wang, F.-L. Meng, Z.-J. Wu, J.-M. Yan, X.-B. Zhang, In Situ Anchoring of Co₉S₈ Nanoparticles on N and S Co-Doped Porous Carbon Tube as Bifunctional Oxygen Electrocatalysts. *NPG Asia Mater.*, 2016, **8**, e308.
- S8. T. Wang, Z. Kou, S. Mu, J. Liu, D. He, I. S. Amiinu, F. Verpoort, 2D Dual-Metal Zeolitic-Imidazolate-Framework-(ZIF)-Derived Bifunctional Air Electrodes with Ultrahigh Electrochemical Properties for Rechargeable Zinc-Air Batteries. *Adv. Funct. Mater.*, 2018, **28**, 1705048.

- S9. C. Tang, B. Wang, H. F. Wang, Q. Zhang, Defect Engineering toward Atomic Co-N_x-C in Hierarchical Graphene for Rechargeable Flexible Solid Zn-Air Batteries. *Adv. Mater.*, 2017, **29**, 1703185.
- S10. C. Y. Su, H. Cheng, W. Li, Z. Q. Liu, N. Li, Z. F. Hou, F. Q. Bai, H. X. Zhang, T. Y. Ma, Atomic Modulation of FeCo-Nitrogen-Carbon Bifunctional Oxygen Electrodes for Rechargeable and Flexible All-Solid-State Zinc-Air Battery. *Adv. Energy Mater.*, 2017, **7**, 1602420.
- S11. T. Zhou, W. Xu, N. Zhang, Z. Du, C. Zhong, W. Yan, Y. Xie, Ultrathin Cobalt Oxide Layers as Electrocatalysts for High-Performance Flexible Zn-Air Batteries. *Adv. Mater.*, 2019, **31**, 1807468.
- S12. Q. Liu, Y. Wang, L. Dai, J. Yao, Scalable Fabrication of Nanoporous Carbon Fiber Films as Bifunctional Catalytic Electrodes for Flexible Zn-Air Batteries. *Adv. Mater.*, 2016, **28**, 3000-3006.
- S13. P. Chen, T. Zhou, L. Xing, K. Xu, Y. Tong, H. Xie, Y. Xie, Atomically Dispersed Iron-Nitrogen Species as Electrocatalysts for Bifunctional Oxygen Evolution and Reduction Reactions. *Angew. Chem. Int. Edit.*, 2017, **129**, 625-629.
- S14. Z. Zhao, Z. Yuan, Z. Fang, J. Jian, J. Li, M. Yang, S. Wang, In Situ Activating Strategy to Significantly Boost Oxygen Electrocatalysis of Commercial Carbon Cloth for Flexible and Rechargeable Zn-Air Batteries. *Adv. Sci.*, 2018, **5**, 1800760.
- S15. Q. Wang, Y. Ji, Y. Lei, Y. Wang, Y. Wang, Y. Li, S. Wang, Pyridinic-N-Dominated Doped Defective Graphene as a Superior Oxygen Electrocatalyst for Ultrahigh-Energy-Density Zn-Air batteries. *ACS Energy Lett.*, 2018, **3**, 1183-1191.
- S16. S. Chen, L. L. Zhao, J. Z. Ma, Y. Q. Wang, L. M. Dai, J. T. Zhang, Edge-Doping Modulation of N, P-Codoped Porous Carbon Spheres for Highperformance Rechargeable Zn-Air Batteries. *Nano Energy*, 2019, **60**, 536-544
- S17. C. Y. Wang, N.-H. Xie, Y. L. Zhang, Z. H. Huang, K. L. Xia, H. M. Wang, S. J. Guo, B.-Q. Xu, Y. Y. Zhang, Silk-Derived Highly Active Oxygen Electrocatalysts for Flexible and Rechargeable Zn-Air Batteries. *Chem. Mater.*, 2019, **31**, 1023-1029.
- S18. A. Pendashteh, J. Palma, M. Anderson, J. J. Vilatela, R. Marcilla, Doping of Self-Standing CNT Fibers: Promising Flexible Air-Cathodes for High-Energy-Density Structural Zn-Air Batteries. *ACS Appl. Energy Mater.*, 2018, **1**, 2434-2439.

19. L. Zhu, D. Zheng, Z. Wang, X. Zheng, P. Fang, J. Zhu, X. Lu, A Confinement Strategy for Stabilizing ZIF-Derived Bifunctional Catalysts as a Benchmark Cathode of Flexible All-Solid-State Zinc-Air Batteries. *Adv. Mater.*, 2018, **30**, 1805268.
- S20. A. Sumboja, M. Lübke, Y. Wang, T. An, Y. Zong, Z. Liu, All-Solid-State, Foldable, and Rechargeable Zn-Air Batteries Based on Manganese Oxide Grown on Graphene-Coated Carbon Cloth Air Cathode. *Adv. Energy Mater.*, 2017, **7**, 1700927.
- S21. H. Zhang, T. Wang, A. Sumboja, W. Zang, J. Xie, D. Gao, J. Wang, Integrated Hierarchical Carbon Flake Arrays with Hollow P-Doped CoSe₂ Nanoclusters as an Advanced Bifunctional Catalyst for Zn–Air Batteries. *Adv. Funct. Mater.*, 2018, **28**, 1804846.
- S22. C. Guan, A. Sumboja, H. Wu, W. Ren, X. Liu, H. Zhang, Wang, J. Hollow Co₃O₄ Nanosphere Embedded in Carbon Arrays for Stable and Flexible Solid-State Zinc-Air Batteries. *Adv. Mater.*, 2017, **29**, 1704117.
- S23. B.-Q. Li, S.-Y. Zhang, B. Wang, Z.-J. Xia, C. Tang, Q. Zhang, A Porphyrin Covalent Organic Framework Cathode for Flexible Zn-Air Batteries, *Energy Environ. Sci.*, 2018, **11**, 1723-1729
- S24. Q. Y. Jin, B. W. Ren, J. P. Chen, H. Cui, C. X. Wang, A Facile Method to Conduct 3D Self-Supporting Co-FeCo/N-Doped Graphenelike Carbon Bifunctional Electrocatalysts for Flexible Solid-State Zinc-Air Battery, *Appl. Catal. B: Environ.*, 2019, **256**, 117887.
- S25. X. P. Han, X. F. Ling, Y. Wang, T. Y. Ma, C. Zhong, W. B. Hu, Y. D. Deng, Spatial Isolation of Zeolitic Imidazole Frameworks-Derived Cobalt Catalysts: From Nanoparticle, Atomic Cluster to Single Atom, *Angew. Chem., Int. Ed.*, 2019, **58**, 5359.
- S26. T. P. Zhou, W. F. Xu, N. Zhang, Z. Y. Du, C. G. Zhong, W. S. Yan, H. X. Ju, W. S. Chu, H. Jiang, C. Z. Wu, Y. Xie, Ultrathin Cobalt Oxide Layers as Electrocatalysts for High-Performance Flexible Zn-Air Batteries, *Adv. Mater.*, 2019, **31**, 1807468.
- S27. Y. Su, Z. Yao, F. Zhang, H. Wang, Z. Mics, E. Cánovas, X. Feng, Sulfur-Enriched Conjugated Polymer Nanosheet Derived Sulfur and Nitrogen co-Doped Porous Carbon Nanosheets as Electrocatalysts for Oxygen Reduction Reaction and Zinc-Air Battery. *Adv. Funct. Mater.*, 2016, **26**, 5893-5902.
- S28. Q. Hu, G. Li, G. Li, X. Liu, B. Zhu, X. Chai, C. He, Trifunctional Electrocatalysis on Dual-Doped Graphene Nanorings-Integrated Boxes for Efficient Water Splitting and Zn-Air Batteries. *Adv. Energy Mater.*, 2019, **9**, 1803867.

- S29. B. B. Huang, X. Hu, Y. C. Liu, W. Qi, Z. L. Xie, Biomolecule-Derived N/S co Doped CNT-Graphene Hybrids Exhibiting Excellent Electrochemical Activities, *J. Power Sources*, 2019, **413**, 408-417.
- S30. J.-J. Lv, Y. L. Li, S. J. Wu, H. Fang, L.-L. Li, R.-B. Song, J. Ma, J.-J. Zhu, Oxygen Species on Nitrogen-Doped Carbon Nanosheets as Efficient Active Sites for Multiple Electrocatalysis, *ACS Appl. Mater. Inter.*, 2018, **10**, 11678-11688.
- S31. Q. Hu, G. M. Li, G. D. Li, X. F. Liu, B. Zhu, X. Y. Chai, Q. L. Zhang, J. H. Liu, C. X. He, Trifunctional Electrocatalysis on Dual-Doped Graphene Nanorings-Integrated Boxes for Efficient Water Splitting and Zn-Air Batteries, *Adv. Energy Mater.*, 2019, **9**, 1803867.
- S32. M. G. Wu, Y. Q. Wang, Z. X. Wei, L. Wang, M. Zhuo, J. T. Zhang, X. P. Han, J. M. Ma, Ternary Doped Porous Carbon Nanofibers with Excellent ORR and OER Performance for Zinc-Air Batteries, *J. Mater. Chem. A*, 2018, **6**, 10918-10925.
- S33. P. Tan, B. Chen, H. Xu, W. Cai, W. He, M. Liu, Ni, M. Co₃O₄ Nanosheets as Active Material for Hybrid Zn Batteries. *Small*, 2018, **14**, 1800225.
- S34. B. Li, X. Ge, F. T. Goh, T. A. Hor, D. Geng, G. Du, Y. Zong, Co₃O₄ Nanoparticles Decorated Carbon Nanofiber Mat as Binder-Free Air-Cathode for High Performance Rechargeable Zinc-air Batteries. *Nanoscale*, 2015, **7**, 1830-1838.
- S35. F. Meng, H. Zhong, D. Bao, J. Yan, X. Zhang, In Situ Coupling of Strung Co₄N and Intertwined N-C Fibers toward Free-Standing Bifunctional Cathode for Robust, Efficient, and Flexible Zn-air Batteries. *J. Am. Chem. Soc.*, 2016, **138**, 10226-10231.
- S36. H. Wu, J. Geng, H. Ge, Z. Guo, Y. Wang, G. Zheng, Egg-Derived Mesoporous Carbon Microspheres as Bifunctional Oxygen Evolution and Oxygen Reduction Electrocatalysts. *Adv. Energy Mater.*, 2016, **6**, 1600794.
- S37. X. Zhu, T. Jin, C. Tian, C. Lu, X. Liu, M. Zeng, S. Dai, In Situ Coupling Strategy for the Preparation of FeCo Alloys and Co₄N Hybrid for Highly Efficient Oxygen Evolution. *Adv. Mater.*, 2017, **29**, 1704091.
- S38. M. Wang, T. Qian, J. Zhou, C. Yan, An Efficient Bifunctional Electrocatalyst for a Zinc-Air Battery Derived from Fe/N/C and Bimetallic Metal-Organic Framework Composites. *ACS Appl. Mater. Inter.*, 2017, **9**, 5213-5221.